Dynamic Mode Decomposition of the Metachronal Paddling Wake

Mitchell P. Ford[1], Arvind Santhanakrishnan[2], and Imraan A. Faruque[3]

Oklahoma State University, Stillwater, OK, 74078, USA

Metachronal paddling is a drag-based propulsion strategy observed in many aquatic arthropods in which a series of paddling appendages are stroked sequentially to form a traveling wave in the same direction as animal motion. Metachronal paddling's relatively high force production makes these organisms highly agile, an attractive potential for bio-inspired autonomous underwater vehicles that is complicated by the lack of reduced order flow structure and dynamics models applicable to vehicle actuation and control design. This study uses particle image velocimetry to quantify the wake of a robot performing metachronal paddling. Then, dynamic mode decomposition is used to identify the frequency modes of the wake, which are used to reconstruct a reduced order model at Reynolds numbers of 32, 160, and 516. The results show that the kinetic energy in the metachronal paddling wake is well modeled using a superposition of the first 5 dynamic modes, and that there is typically little change in the reconstruction error when the reconstruction is performed with a higher number of dynamic modes. The low order paddling models identified using this method can be used to identify the physical mechanisms that differentiate metachronal paddling from synchronous paddling, and to develop control strategies to modulate these motions in bio-inspired autonomous underwater vehicles.

I. Nomenclature

AUV	=	Autonomous Underwater Vehicle
d, ∂	=	Derivative operator
DMD	=	Dynamic Mode Decomposition
$\hat{e}$	=	Reconstruction error in kinetic energy
E	=	Kinetic energy
f	=	Paddling stroke frequency
Fr	=	Froude number
G	=	Inter-paddle spacing (Gap)
I	=	Identity matrix
j	=	Complex number $\sqrt{-1}$
L	=	Paddle length
λ, Λ	=	Eigenvalue, Eigenvalue matrix
∇	=	Gradient operator
ν	=	Kinematic viscosity
p	=	Pressure
PIV	=	Particle Image Velocimetry
Φ	=	Dynamic mode
Re	=	Reynolds number
ρ	=	Fluid density
Σ	=	Singular value matrix

---

[1] Graduate Research Associate, School of Mechanical and Aerospace Engineering.
[2] Associate Professor, School of Mechanical and Aerospace Engineering.
[3] Assistant Professor, School of Mechanical and Aerospace Engineering, AIAA Member.

$\tilde{\Sigma}$	=	Eigendecomposition matrix
t	=	Time
θ	=	Paddling stroke amplitude
u	=	Horizontal component of fluid velocity
$\bar{u}$	=	Fluid velocity vector
$\hat{u}$	=	Reconstructed fluid velocity
U	=	Left singular vector matrix
v	=	Vertical component of fluid velocity, eigenvector matrix
V	=	Data matrix
W	=	Right singular vector matrix
ω_z	=	Transverse component of vorticity vector
x	=	Horizontal axis direction
y	=	Vertical axis direction

II. Introduction

Metachronal paddling is a drag-based locomotion strategy that is commonly used by numerous species of aquatic and semi-aquatic organisms. The metachronal swimming stroke is performed by organisms that have multiple swimming appendages aligned along the body axis, where each appendage is stroked sequentially, with a small phase lag between the movement of adjacent appendages. In marine crustaceans with 5 pairs of swimming legs, this inter-leg phase lag is commonly about 15-18% of the total cycle time [1]. Of particular importance to oceanography and marine ecology are species that form large schools or swarms, such as Antarctic krill, due to their hypothesized role in biogenic ocean mixing [2]. Much work has been done on the swimming performance of individual paddling organisms [3-5], a recent study has examined the preferred schooling orientations of krill in a laboratory aquarium [6], and a few studies have begun to examine how organisms might be able to sense and respond to their hydrodynamic environments [7-8]. All this research helps build an understanding of the behavior of individual organisms but does not explain how or why individuals in a group choose to interact in the ways that they do.

Work is being done to develop highly agile autonomous underwater vehicles (AUVs) and drag-based propulsion strategies such as metachronal paddling are ideal for this purpose. Identification of the fluid dynamic modes in the wake of individual paddling swimmers can help to inform the understanding of collective decision making and can be used to help in the design of swarm operation of these autonomous underwater vehicles. By applying dynamic mode decomposition (DMD) to identify the frequency modes in the paddling wake, it may be possible to identify particular flow structures that can be sensed by individual vehicles in a swarm for autonomous swarm organization. Particular sensory elements will need to be developed for these vehicles that can read hydrodynamic cues in the paddling wake in order to coordinate these collective motions of multiple autonomous underwater vehicles. To test this, particle image velocimetry (PIV) was performed on the wake of a robotic model that was programmed to perform a metachronal paddling motion, and DMD was performed on the paddling wake to determine whether a low-order linear approximation can be used to accurately model the paddling wake.

Dynamic mode decomposition, famously introduced by Schmid [11], is a numerical method that allows for the extraction of frequency modes and coherent structures from flow field data [12]. An advantage of the DMD method is that it provides a way to characterize the most important flow structures [13], which can then be used to identify physical mechanisms and develop control strategies. DMD has been widely applied to wake flows and can be applied for both uniform and nonuniform time sampling [14]. A systematic comparison of DMD to other common data decomposition methods is given in [15]. These identified frequency modes can be determined in the absence of any prior knowledge of the physics of the problem and can help determine the frequencies of the dominant flow structures, for maximum efficiency in flow modeling. Researchers are hopeful that as DMD continues to rise in popularity, advances will make it applicable for real-time frequency mode identification and control for fluid flow applications [15].

III. Methods and Approach

A. Experimental Methods

A multi-appendage paddling robot was developed to investigate the metachronal paddling propulsion mechanism. The design of the system and experimental procedures are detailed in [4]. The model was designed to mimic metachronal propulsion as seen in crustaceans such as Antarctic krill and used an inter-paddle spacing (ratio of gap between paddles, G, to paddle length, L) of G/L=0.7. Previous work [10] has shown that close spacing of the paddles

2

(G/L<1.0) results in increased propulsive performance (increased fluid transport, increased swimming speed of the robot) relative to paddles that are spaced far apart. The model was programmed to perform a sinusoidal paddle stroke, with a stroke amplitude of $\theta = 90°$ and a stroke frequency of $f = 1.5\ Hz$. The paddles had length $L = 76.2\ mm$, with a hinge located halfway along the length that allowed them to fold in one direction in order to reduce the surface area perpendicular to the flow during the recovery stroke. The Reynolds number based on mean paddle tip speed can be defined as:

$$Re = \frac{2f\theta L^2}{\nu} \tag{1}$$

The model was operated in three different fluids, with varying viscosities. The fluids were mixtures of glycerin and water in different concentrations, with kinematic viscosities of $\nu = 860\ \frac{mm^2}{s}$, $\nu = 172\ \frac{mm^2}{s}$, and $\nu = 53\ \frac{mm^2}{s}$, which resulted in average paddle-tip speed based Reynolds numbers of $Re = 32$, $Re = 160$, and $Re = 516$, respectively. A diagram of the experimental setup as well as prescribed and measured paddle kinematics are shown in **Figure 1**.
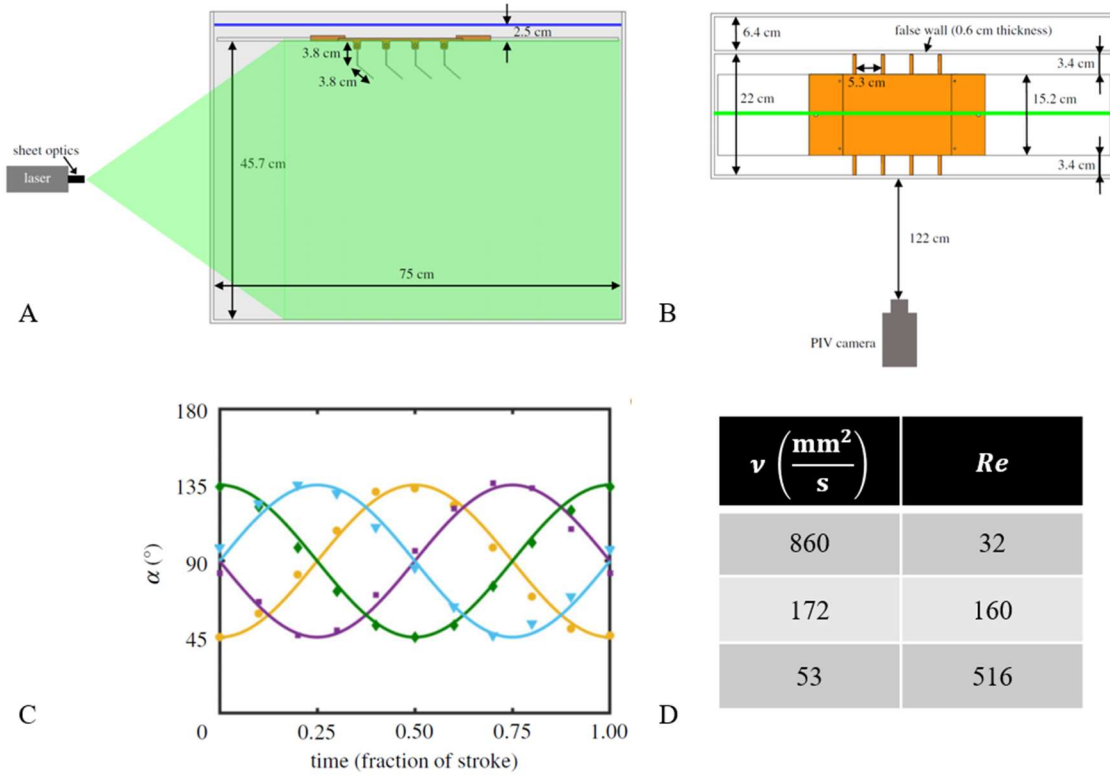

Fig. 1 Experimental setup used in this study. (A) Front view of experimental setup. (B) Top view. (C) Paddle kinematics with phase lag of 25% of total cycle time. α represents paddle root angle. (D) kinematic viscosity of each fluid and resulting Reynolds numbers. Reproduced under CC-BY-4.0 from Ford et al. 2019 [4].

Particle image velocimetry experiments were performed on the robotic model at a rate of 15 double-frame images per second, which resulted in 10 PIV vector fields calculated per paddling stroke. An Imager sCMOS camera (LaVision GmbH, Göttingen, Germany) and a double-pulsed Nd:YAG laser (Gemini 200-15, New Wave Research, Fremont, CA, USA) were used for the recording, and PIV calculation was performed in DaVis 8.3 (LaVision GmbH, Göttingen, Germany). The data used for the analysis here, along with further details about the data acquisition and PIV processing methods are previously published in [4]. The previously published velocity field data was read into MATLAB R2021a (MathWorks inc., Natick, NJ), and run through the DMD as described in the next section.

B. Computational Methods

For a 2D velocity field size $m \times n$ with time history of length N, given by $\vec{u}(x, y, t) = u(x, y, t)\hat{\imath} + v(x, y, t)\hat{\jmath}$, the velocity field data can be written as a 2D matrix given by

3

$$V_1^N = \begin{bmatrix} u(x_1,y_1,t_1) & \dots & u(x_1,y_1,t_N) \\ u(x_2,y_1,t_1) & \dots & u(x_2,y_1,t_N) \\ & \vdots & \\ u(x_m,y_n,t_1) & \dots & u(x_m,y_n,t_N) \\ v(x_1,y_1,t_1) & \dots & v(x_1,y_1,t_N) \\ & \vdots & \\ v(x_m,y_n,t_1) & \dots & v(x_m,y_n,t_N) \end{bmatrix} \tag{2}$$

Since the fluid motion in the metachronal paddling system is periodically forced by the paddle motion and incorporates periodic shed wakes, it is convenient to apply dynamic modal decomposition (DMD) to paddling stroke phase-synchronized instances of the flow field. This quasi-steady approach can be used to capture the cycle-to-cycle variation of the propulsive wake. For this study, the time point $\frac{t}{T} = 0.5$ was chosen for the DMD processing, corresponding to the to the configuration indicated at 0.5 on the x-axis of the plot in **Fig. 1C**. Physically, this time point occurs just as the rightmost paddle in **Fig. 1A** completes its thrust-generating power stroke. Future work will consider additional timepoints. The first step in DMD is to calculate the singular value decomposition (SVD) of the matrix V_1^{N-1}, given by

$$V_1^{N-1} = U\Sigma W^T, \tag{3}$$

where Σ is a diagonal matrix of singular values, and the columns of the matrices U and W are the left-hand and right-hand singular vectors, respectively. The SVD modes are not unique. To overcome this limitation, it is possible to define the dynamic mode decomposition by taking performing the eigendecomposition on the square matrix $\tilde{\Sigma}$, defined as

$$\tilde{\Sigma} = U^* V_1^{N-1} W^T \Sigma^{-1}. \tag{4}$$

While the velocity matrix V_1^{N-1} is not square, $\tilde{\Sigma}$ is, and therefore the eigendecomposition can be performed. The decomposition of the matrix $\tilde{\Sigma}$ is performed according to the following, where the diagonalized eigenvalue matrix is given by $\Lambda = \lambda I$, and the eigenvector matrix is given by v:

$$\tilde{\Sigma} v = v\Lambda. \tag{5}$$

Thus the dynamic modes Φ of the system are

$$\Phi = V_1^{N-1} W \Sigma^{-1} v. \tag{6}$$

A low-order linear reconstruction of the vector field can be performed using a superposition of the first i dynamic modes Φ_i. This is done by performing a linear-least-squares fit ϕ_i of Φ_i to the last column of V_1^N, corresponding to the instant $t = N$:

$$\Phi_i \phi_i = V^N \tag{7}$$

The flow field reconstruction is then based on a fit of the velocity field. The quality of the low-order reconstruction can be calculated based on the total error in the kinetic energy of the reconstruction. The total kinetic energy in the flow field per unit width for 2D velocity data can be calculated according to the equation:

$$E = \iint \frac{1}{2} \rho |\vec{u}(x,y)|^2 \, dx \, dy \tag{8}$$

And the reconstruction error in the kinetic energy data was quantified by:

$$e = \frac{\iint \left[(u(x,y) - u_{DMD}(x,y))^2 + (v(x,y) - v_{DMD}(x,y))^2 \right] \cdot dx \cdot dy}{\iint [u(x,y)^2 + v(x,y)^2] \cdot dx \cdot dy} \cdot 100\%, \tag{9}$$

4

where u and v are the velocity components of the experimental data, and u_{DMD} and v_{DMD} are the velocity components from the data reconstructed from the DMD modes. The method in Eqns. (2)-9 was implemented in MATLAB R2021a (version 9.10, MathWorks Inc., Natick, MA.).

IV. Results and Discussion

Singular value decomposition was performed as a step in the calculation of the dynamic modes. The singular values are shown in **Fig. 2**. The maximum singular values and the sum of all values are shown in Table 1.

Table 1. Singular values as a function of Reynolds number

Re	Max singular value σ	Sum of 30 singular values
32	110	127
160	176	265
516	163	432

The sum of singular values suggests there is more energy transfer within the higher Reynold's number flow, and a low rank decomposition is more direct for lower speed flows. This finding is consistent with the physical understanding from the governing non-dimensional form of the incompressible Navier-Stokes equation with no body forces, given below

$$\frac{\partial u'}{\partial t'} + (u' \cdot \nabla')u' = -\nabla'p' + \frac{1}{Re}\nabla'^2 u' \tag{10}$$

The Navier-Stokes equation behaves linearly at very low Reynolds numbers and becomes increasingly nonlinear as Reynolds number increases. We expect higher Reynolds number flows will require a significantly greater number of linear modes to accurately capture the dynamics at higher values of Re.
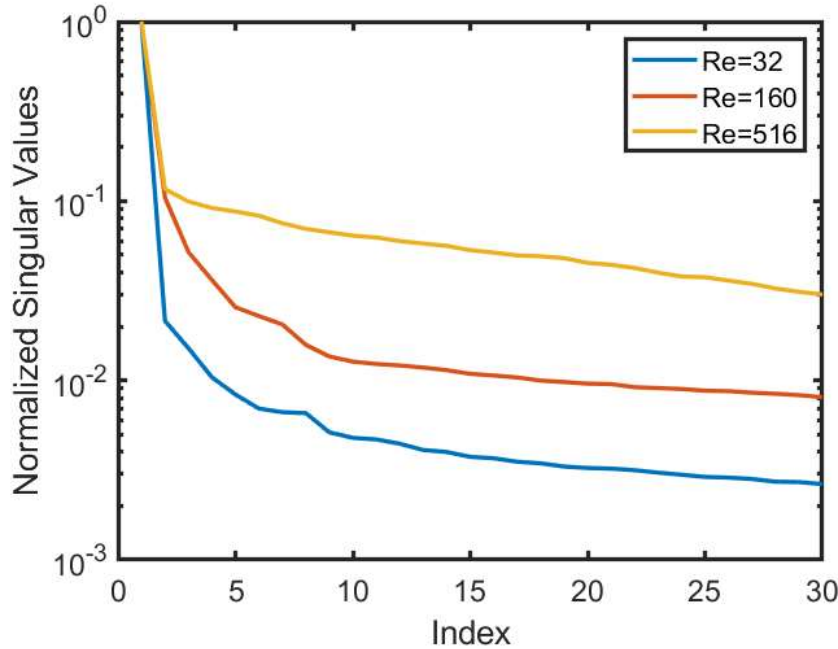

Fig. 2 Normalized singular values Σ in descending order.

The dynamic modes of the system were calculated in MATLAB, which showed alternating modes of the same magnitude but opposite directions, and that these modes were associated with complex conjugate eigenvalue pairs. For this reason, only the odd modes are shown here, with mode 1 representing the mean value of the PIV time-series, and subsequent modes representing periodic cycle-to-cycle variation in the flow field. The first few dynamic modes of the paddling system for the given kinematics (25% phase lag, 90° stroke amplitude) are shown in **Fig. 3**. Mode 1 appears to show coherent structures in the vorticity field, representing paddle tip vortices and the mean shear flow. For $Re = 32$ and $Re = 160$, subsequent modes after the 1st mode show greater vorticity concentration

near the paddle tips than anywhere else in the flow, which likely represents noise in the experimental data caused by glare from the laser sheet reflecting off of the acrylic paddles. However, the relatively greater vorticity components in the far-field at $Re = 160$ as compared to $Re = 32$ may indicate that there is some physical component to the cycle-to-cycle variation in the flow fields that is above and beyond the experimental noise likely represented by the far-field vorticity contours at $Re = 32$. In contrast to the other two Reynolds number cases, the vorticity modes at $Re = 516$ show clearly defined regions of vorticity that are likely to correspond to periodic differences in the metachronal paddling wake. Despite the paddles repeatedly making the same motion, the wake varies over time. A likely cause of this variation is that there is less viscous dissipation of fluid momentum at higher Reynolds numbers. This effect results in vortices shed from previous paddling strokes remaining non-negligible rather than decaying quickly. The slowly decaying vortical structures can interact with the subsequent paddling strokes in different ways. This interaction results in a time-varying wake despite the periodic forcing of the flow and can have significance for marine ecology and engineering of autonomous underwater vehicles. A wake that does not consistently have the same vorticity signature would require a more complex flow sensing system for schooling in animals and swarm operation in engineered vehicles at larger Reynolds numbers.
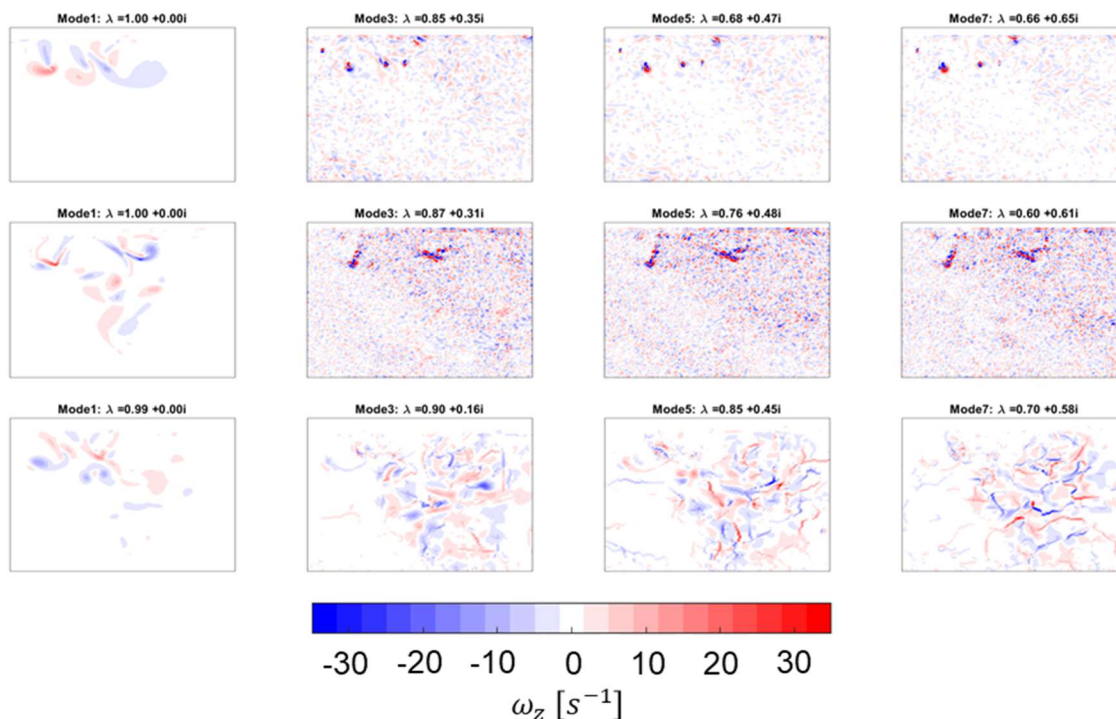

Fig. 3 Vorticity fields corresponding to the first 4 odd dynamic modes each Reynolds number. First row: Re=32. Second row: Re=160. Third row: Re=516.

The dynamic modes of the system were used as the basis for a reduced-order model of the paddling wake. During the experiments, the robotic model was run for 100 paddling cycles to develop a steady, periodic wake based on the momentum and momentum flux values as seen in [4]. After this steady periodic wake state was achieved, data was recorded for 31 cycles. The first 30 paddling stroke cycles were used to calculate the DMD modes, which were then fit to the 31st cycle data for comparison to determine how well the low-order reconstruction fit the experimental data. The experimental PIV data, along with low-order reconstructions based on the first dynamic mode, and on the first 5 distinct modes are shown for each Reynolds number in **Fig. 4**. For the lowest Reynolds number ($Re = 32$), there is virtually no difference between the experimental data and the two linear approximations of the data, so a first order approximation of the wake works just as well as a 5th order approximation. However, increasing the Reynolds number increases non-linear interactions in the fluid physics (Equation 10), which should require a higher-order linear approximation to accurately model the flow physics. At $Re = 160$, There are some visual differences in the wake vorticity between the three plots (**Fig. 4**), but the differences in velocity magnitude are small, and the difference in vorticity is primarily far from the core of the wake jet. At $Re = 516$, there are larger differences in the wake velocity between the data and both the first and fifth-order linear reconstructions of the fluid

wake. This indicates that there is much greater cycle-to-cycle variation in the wake. Despite the differences between the data and the reconstructions far from the wake core, the overall flow field looks fairly similar even using just a first order linear approximation for the reconstruction. In order to quantify how well the reconstructions matched the wake, the total error in the kinetic energy of the reconstructions were calculated using Equation 9.
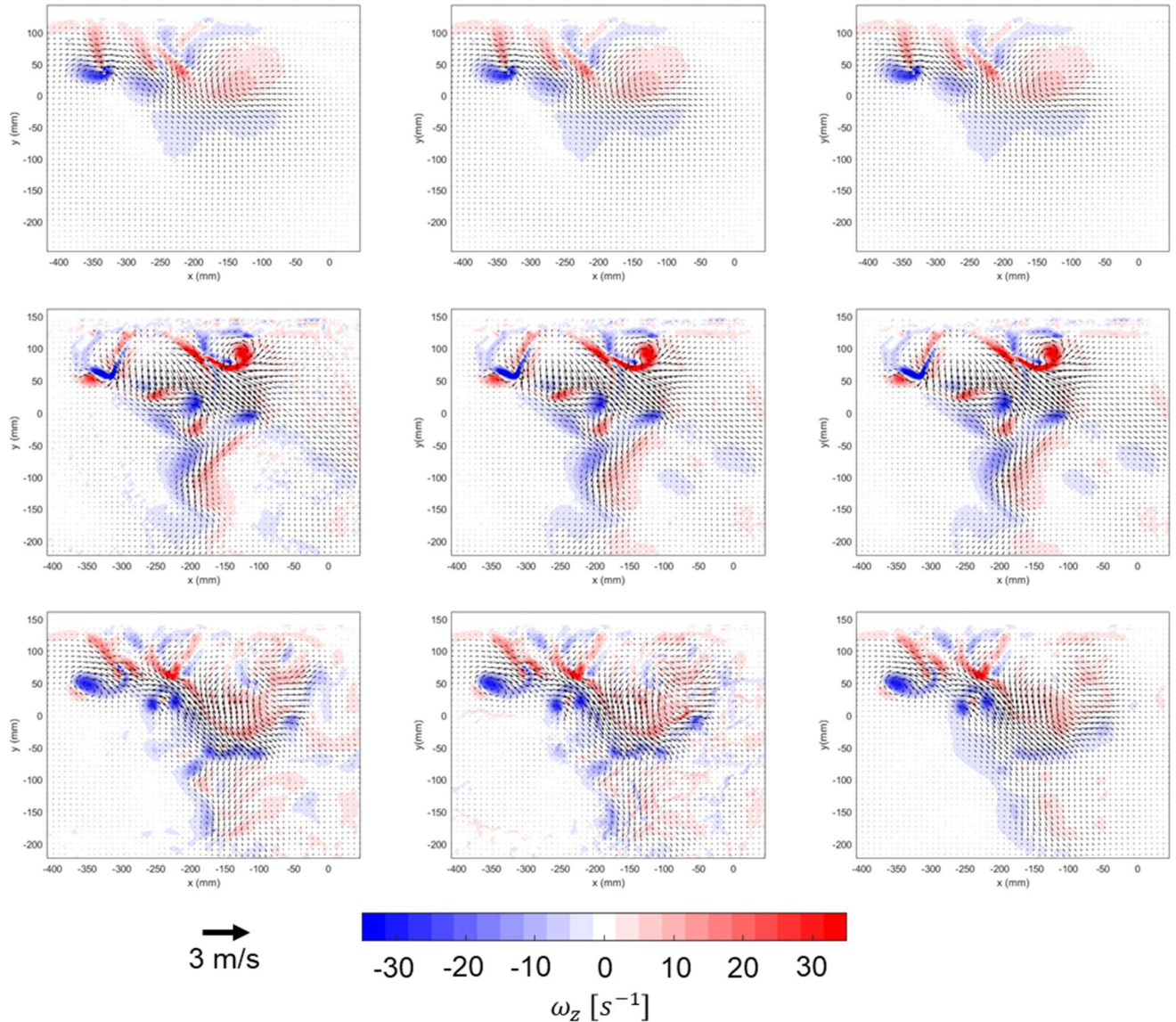

Fig. 4 PIV velocity and vorticity fields (left) compared with low-order reconstructions using the first 5 modes (center) and the first mode only (right). The Reynolds numbers are $Re = 32$ (top), $Re = 160$ (center), and $Re = 516$ (bottom).

The total amount of error in the kinetic energy of the reconstructed flow field is shown in Fig. 5, for varying number of modes used for the flow field reconstruction at each Reynolds number. For the lowest Reynolds number, $Re = 32$, there is little difference made in the kinetic energy reconstruction error by adding more modes beyond the first mode. The first mode captures more than 99.92% of the total kinetic energy, with an error slightly less than 0.077%. The total kinetic energy for this case was 2.04 J/m. At higher Reynolds numbers, the reconstruction error in the kinetic energy increased. For $Re = 160$, the total kinetic energy in the field of view from the PIV experiments was 5.38 J/m, with the reconstruction error decreasing from 2.11% to 1.10% as the number of modes used for reconstruction increased from 1 to 29. At $Re = 516$, the reconstruction error increased drastically to 10.4% when using only the first mode for reconstruction, dropped to 4.38% when reconstructed using the first 15 modes, and finally to 1% when the first 29 modes were used in the flow field reconstruction. So as Reynolds number increases,

it is likely necessary to use a more complex sensory array to detect the wake of an individual paddler, but at these Reynolds numbers, a low order model should do nicely due to the large amount of energy information contained in the first few modes. From **Fig. 4**, the mean flow occurs near the same location and with similar intensity in both the first and fifth order reconstructions of the paddling wake at each Reynolds number. Since the wake structure and energy content from the low-order model is relatively close to that from the experimental data, it means that animals that swim in groups using metachronal paddling, and engineered AUVs attempting to follow a formation leader could require only low-order feedback control that responds to low-speed, high-intensity fluctuations in the paddling wake. This simplification would allow them to respond to changes in the wake that correspond primarily to the reorientation of the wake jet due to the swimming motion of other individuals in the swarm, rather than the fluctuations in the flow field that are due to nonlinearities of the flow physics.
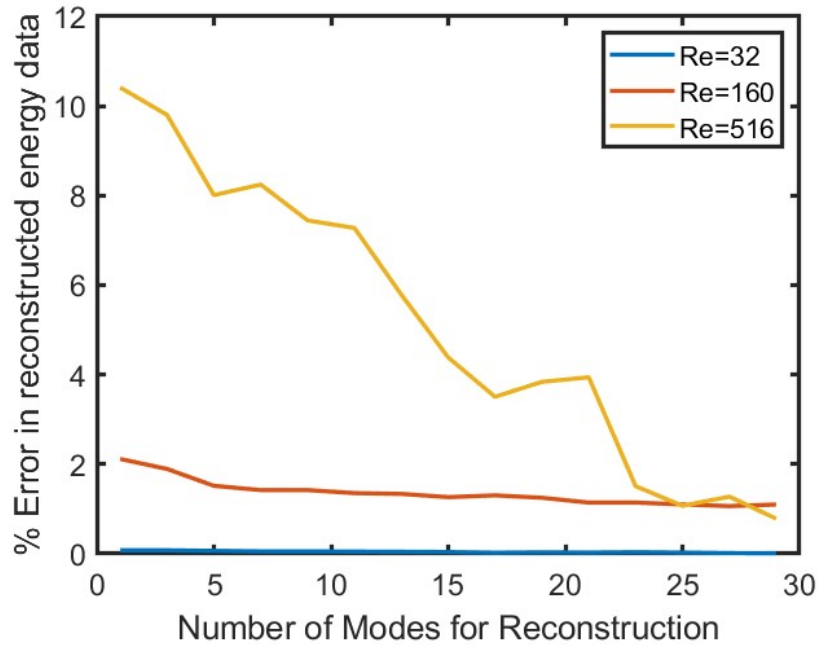

Fig. 5 Reconstruction error (calculated according to equation 9) versus number of modes used for reconstruction.

V. Conclusion

In this study, it was found that a low-order linear model does a good job of capturing the energy content of the metachronal paddling wake. Dynamic Mode Decomposition (DMD) was used to determine cycle-to-cycle variations in the periodic wake of a metachronally paddling robot, and it was found that up to $Re = 516$, a linear reconstruction using only the first dynamic mode captures nearly 90% of the energy in the wake flow. The results of this study can be combined with information on the coherent wake structures to develop simple linear models for swarm operation that could be used to control bio-inspired Autonomous Underwater Vehicles or applied to describe the motion of marine organisms in a school.

Acknowledgments

References

[1] Murphy, D. W., Webster, D. R., Kawaguchi, S., King, R., and Yen, J., "Metachronal swimming in Antarctic krill: Gait kinematics and system design," *Mar. Biol*, Vol. 158, No. 11, 2011, pp. 2541–2554. https://doi.org/10.1007/s00227-011-1755-y

[2] Katija, K., Dabiri, J. O., "A viscosity-enhanced mechanism for biogenic ocean mixing," *Nature*, Vol. 460, No. 7255, 2009, pp. 624-626. https://doi.org/10.1038/nature08207

[3] Alben, S., Spears, K., Garth, S., Murphy, D. W. and Yen, J., "Coordination of multiple appendages in drag-based swimming," *J. R. Soc. Int*. Vol. 7, No. 52, 2010, pp. 1545–1557. https://doi.org/10.1098/rsif.2010.0171

[4] Ford, M. P., Lai, H. K., Samaee, M., and Santhanakrishnan, A., "Hydrodynamics of metachronal paddling : effects of varying Reynolds number and phase lag," *R. Soc. Open Sci.* [online journal]*, Vol. 6, No. 191387, 2019. https://doi.org/10.1098/rsos.191387

[5] Ford, M. P., Ray, W. J., DiLuca, E. M., Patek, S. N., and Santhanakrishnan, A., "Hybrid Metachronal Rowing Augments Swimming Speed and Acceleration via Increased Stroke Amplitude," *Integr. Comp. Biol*, Vol. 61, No. 5, 2021, pp. 1619–1630. https://doi.org/10.1093/icb/icab141

[6] Murphy, D. W., Olsen, D., Kanagawa, M., King, R., Kawaguchi, S., Osborn, J., Webster, D. R., and Yen, J., "The three dimensional spatial structure of Antarctic krill schools in the laboratory," *Scientific Reports* [online journal], Vol. 9, No. 381, 2019. https://doi.org/10.1038/s41598-018-37379-9

[7] Fields, D. M., and Yen, J., "The escape behavior of marine copepods in response to a quantifiable fluid mechanical disturbance," *J. Plankton Res.* Vol. 19, No. 9, 1997, pp. 1289-1304. https://doi.org/10.1093/plankt/19.9.1289

[8] Gazzola, M., Tchieu, A. A., de Brauer, A., and Koumoutsakos, P., "Learning to school in the presence of hydrodynamic interactions," *J. Fluid Mech*., Vol. 789, 2016, pp. 726-749. https://doi.org/10.1017/jfm.2015.686

[9] Ford, M. P., and Santhanakrishnan, A., "On the role of phase lag in multi-appendage metachronal swimming of euphausiids," *Bioinspir. Biomim.* [online journal], Vol. 16, No. 066007, 2021. https://doi.org/10.1088/1748-3190/abc930

[10] Ford, M. P., and Santhanakrishnan, A., "Closer appendage spacing augments metachronal swimming speed by promoting tip vortex interactions," *Integr. Comp. Biol.* Vol. 61, No. 5, 2021, pp. 1608-1618. https://doi.org/10.1093/icb/icab112

[11] Schmid, P. J., "Dynamic mode decomposition of numerical and experimental data," *J. Fluid Mech*. Vol. 656, 2010, pp. 5-28. https://doi.org/10.1017/S0022112010001217

[12] Chen, K. K., Tu, J. H., and Rowley, C. W., "Variants of Dynamic Mode Decomposition: Boundary Condition, Koopman, and Fourier Analyses," *J. Nonlinear Sci.* Vol. 22, 2012, pp. 887-915. https://doi.org/10.1007/s00332-012-9130-9

[13] Schmid, P. J., Li, L., Juniper, M. P., and Pust, O., "Applications of the dynamic mode decomposition,", *Theor. Comput. Fluid Dyn,* Vol. 25, 2011, pp. 249-259. https://doi.org/10.1007/s00162-010-0203-9

[14] Tu, J. H., Rowley, C. W., Luchtenburg, D. M., Brunton, S. L., and Kutz, J. N., "On dynamic mode decomposition: Theory and applications," *J. Comput. Dyn.* Vol. 1, No. 2, 2014, pp. 391-421. https://doi.org/10.3934/jcd.2014.1.391

[15] Taira, K., Brunton, S.L., Dawson, S. T. M., Rowley, C. W., Colonius, T., McKeon, B. J., Schmidt, O. T., Gordeyev, S., Theofilis, V., and Ukeiley, L. S., "Modal analysis of fluid flows: an overview," *AIAA Journal*. Vol. 55, No. 12, 2017, pp. 4013-4041. https://doi.org/10.2514/1.J056060